

Liver Aging and Pseudocapillarization in a Werner Syndrome Mouse Model

Victoria C. Cogger,^{1,*} Dmitri Svistounov,^{1,*} Alessandra Warren,¹ Svetlana Zykova,¹ Richard G. Melvin,² Samantha M. Solon-Biet,^{1,3} Jennifer N. O'Reilly,¹ Aisling C. McMahon,¹ J. William O. Ballard,² Rafa De Cabo,⁴ David G. Le Couteur,¹ and Michel Lebel⁵

¹Centre for Education and Research on Aging and ANZAC Medical Research Institute, University of Sydney and Concord Hospital, New South Wales, Australia.

²School of Biotechnology and Biomolecular Science, University of New South Wales, Sydney, Australia.

³School of Biological Sciences, University of Sydney, New South Wales, Australia.

⁴Experimental Gerontology Section, Translational Gerontology Branch, National Institute on Aging, National Institutes of Health, Baltimore, Maryland.

⁵Centre de Recherche en Cancérologie de l'Université Laval, Hôpital Hotel-Dieu de Québec, Canada.

*These authors contributed equally to this work.

Address correspondence to Victoria C. Cogger, PhD, Centre for Education and Research on Aging and ANZAC Medical Research Institute, University of Sydney and Concord Hospital, Gate 3, Hospital Road, Concord Hospital, Sydney, NSW 2139, Australia.

Email: victoria.cogger@sydney.edu.au

Werner syndrome is a progeric syndrome characterized by premature atherosclerosis, diabetes, cancer, and death in humans. The knockout mouse model created by deletion of the RecQ helicase domain of the mouse *Wrn* homologue gene (*Wrn*^{Δhel/Δhel}) is of great interest because it develops atherosclerosis and hypertriglyceridemia, conditions associated with aging liver and sinusoidal changes. Here, we show that *Wrn*^{Δhel/Δhel} mice exhibit increased extracellular matrix, defenestration, decreased fenestration diameter, and changes in markers of liver sinusoidal endothelial cell inflammation, consistent with age-related pseudocapillarization. In addition, hepatocytes are larger, have increased lipofuscin deposition, more frequent nuclear morphological anomalies, decreased mitochondria number, and increased mitochondrial diameter compared to wild-type mice. The *Wrn*^{Δhel/Δhel} mice also have altered mitochondrial function and altered nuclei. Microarray data revealed that the *Wrn*^{Δhel/Δhel} genotype does not affect the expression of many genes within the isolated hepatocytes or liver sinusoidal endothelial cells. This study reveals that *Wrn*^{Δhel/Δhel} mice have accelerated typical age-related liver changes including pseudocapillarization. This confirms that pseudocapillarization of the liver sinusoid is a consistent feature of various aging models. Moreover, it implies that DNA repair may be implicated in normal aging changes in the liver.

Key Words: Sinusoid—Endothelium—Mitochondria—Electron microscopy—Seahorse analyzer.

Received August 1, 2013; Accepted September 6, 2013

Decision Editor: Placido Navas, PhD

OLD age is associated with increased vulnerability, susceptibility to disease, and disability and is the major independent risk factor for most diseases of the Western world including atherosclerosis, cancer, and arthritis as well as prototypical aging diseases such as dementia and osteoporosis (1). Although the aging process is the main determinant of disease beyond the third decade of life (2), our understanding of how old age predisposes to disease remains rudimentary (3). It has been recognized that the liver may be central to the aging process because it plays a pivotal role in many metabolic and detoxification processes that impact on aging and disease susceptibility in the rest of the body.

The liver had long been thought to be preserved from any significant age-related changes. A growing body of evidence, however, shows that older age is associated with marked changes in all cells of the liver (4,5) and particularly

the liver sinusoidal endothelial cells (LSECs) (6). These age-related changes to the LSEC, called pseudocapillarization, are now known to affect directly hepatic metabolism through inhibiting transfer of substances such as lipids and drugs between the blood and liver parenchyma (7,8). In particular, fenestrations, which are transcellular pores that facilitate transfer of substrates across the LSEC, are reduced in both number and diameter in old age in all species yet reported including humans.

Werner Syndrome (WS) is a human autosomal recessive progeric condition that causes the premature onset of clinical signs of aging, such as cardiovascular disease, cancer, and osteoporosis. It is caused by a mutation of the WRN (RECQL2) gene, which encodes a RecQ family 3'-5' DNA helicase protein that also has a 3'-5' exonuclease domain at its N-terminus region (9,10). The protein is involved in DNA recombination, transcription, repair, and telomere

maintenance (11–13). The life expectancy of a person with WS has climbed from 46 years in the 1990s (14) to 55 years due to better medical care (15) and the introduction of anti-diabetic drugs, underlining again the abnormal metabolic profile of these patients (16).

A number of mouse models of WS have been developed (17–19). In this report, we investigate the *Wrn* helicase mutant mice, *Wrn*^{Δhel/Δhel}, which lack the helicase unit of the *Wrn* gene. Although these mice do not develop a severe aging phenotype, they do exhibit many of the WS phenotypes including hypertriglyceridemia, insulin resistance, an increased incidence of cancer, and a decreased life expectancy (20,21). Previously, we have shown that vitamin C supplementation and resveratrol treatment have beneficial effects on the health and/or life span of these *Wrn*^{Δhel/Δhel} mice. Many of these effects were mediated in part by the liver, and we believe that the liver sinusoidal endothelium played an integral role (22,23). Hence, the aim of this study was to systematically investigate the morphology, gene expression, and function of the liver sinusoidal endothelium as well as the hepatocytes in *Wrn*^{Δhel/Δhel} mice and to further evaluate these mice for use in aging liver studies.

METHODS

Homozygous WRN helicase transgenic (*Wrn*^{Δhel/Δhel}) on a C57Bl6 background and C57Bl6 wild-type (WT) control male mice aged 4–7 months and 14–16 months were used for all parameters in this study, with the exception of the microarray analysis where 3- to 4-month-old and 13- to 14-month-old animals were used. Control C57Bl6 mice were bred independently. All animals were housed in the Molecular Physiology unit at the ANZAC Research Institute and allowed free access to water and commercial pellets. This study was approved by the Sydney South Western Area Health Service Animal welfare committee.

Biochemical Parameters

Basic liver function tests (alanine transaminase and aspartate transaminase) were measured in plasma blood with the Roche Hitachi cobas 8000 Modular Analyzer (Roche Diagnostics, Indianapolis, IN) in the Biochemical Department of Concord Hospital ($n = 4$ mice per age group and genotype). Plasma insulin levels were measured using the Ultrasensitive Mouse Insulin ELISA Kit (Alpcor Diagnostics, Salem, New Hampshire) ($n = 4$ mice per age group and genotype).

Morphological and Ultrastructural Studies

For liver morphology studies, liver perfusion was performed as described previously (24). In addition, one lobe was ligated and placed in 4% phosphate-buffered

paraformaldehyde for histology and immunohistochemistry prior to introduction of fixative for electron microscopy analysis.

Following fixation, liver samples for transmission electron microscopy were embedded in Spurrs resin, sectioned, and examined using a Philips CM10 transmission electron microscope. Liver morphology was assessed for mitochondrial density, lipid deposition, nuclei morphology, and fibrotic changes. Liver pieces for scanning electron microscopy were prepared as previously described (7), and fenestration density and size were examined using a JEOL 6380 scanning electron microscope. Five mice per age group and genotype were analyzed by electron microscopy techniques. Not less than 10 hepatocytes were analyzed per animal, and at least 350 mitochondria per animal were analyzed to calculate mitochondria size and number. Nuclei area was excluded from hepatocyte area for calculation of mitochondrial density.

For histology, liver samples were embedded in paraffin, sectioned at 4 μ m, and stained with hematoxylin and eosin for gross morphology or Sirius red, a stain for liver collagen deposition, a marker of liver fibrosis (25).

Immunohistochemistry was used to determine the expression of LYVE1, perlecan, and ICAM 1 (antigens expressed on LSECs and extracellular matrix) on frozen sections, and the expression of F4/80 (Kupffer cell antigen) was analyzed on paraffin sections.

Endogenous peroxidase was blocked with 0.3% hydrogen peroxide. The primary antibodies, which were applied for 1 hour were LYVE1 (ALY7 eBioscience, 1:200), perlecan (A7L6 -Neomarkers, 1:200), ICAM-1, and F4/80 (kindly provided by P.Bertolino, 1:10). Sections were then treated with anti-rat biotinylated secondary antibody and ExtrAvidin peroxidase (Sigma). 3,3'-Diaminobenzidine was used to reveal peroxidase activity. The immunohistochemistry staining was rated blindly and independently. Staining was rated between zero and three for the intensity of staining in the periportal sinusoids, pericentral sinusoids, portal vein, and central veins ($n = 5$ mice per age group and genotype) were analyzed using these histological and immunohistochemical techniques.

Microarray Studies

For gene expression study, total RNA was isolated from hepatocytes and LSEC isolated from 3- to 4-month-old and 13- to 14-month-old *Wrn*^{Δhel/Δhel} and WT mice (3 mice per age and genotype) using RNAeasy (Qiagen). Cells were obtained after liver perfusion with liberase (Roche), Percoll gradient separation of nonparenchymal cells and subsequent removal of Kupffer cells by selective adherence. Amplified cRNA was hybridized onto Illumina. SingleColor.MouseWG-6 v2.0 Whole-Genome Expression BeadChip containing 45,280 probes for 30,853 genes. Raw fluorescence intensity values were quantile normalized with

The BeadStudio software (Illumina Inc.) and log-transformed prior to two-way ANOVA analysis with Benjamini-Hochberg false discovery rate correction.

Seahorse Mitochondrial Studies

Mitochondrial respiration and oxidation in the livers were assessed using a Seahorse Extracellular Flux Analyzer. Substrates studied were glutamate/malate and succinate, and responses to ADP, Oligomycin, FCCP, and Antimycin A were quantified ($n = 4$ per genotype, age 4–7 months). Data were extracted from Excel spreadsheets using “R” and respiration states calculated using the point-to-point calculations.

Mitochondrial DNA Studies

For quantification of mitochondrial DNA, total DNA was extracted from isolated hepatocytes from four groups of mice using DNeasy kit (Qiagen) ($n = 3$ mice per age and genotype).

Two mitochondria-encoded genes (NADH dehydrogenase subunit 5 and ATP synthase F0 subunit 6) and one nuclear-encoded gene (transferrin receptor, which is a single copy nuclear gene) were quantified by RealTime PCR using TaqMan chemistry. Amplification efficiency was calculated from standard curves for each gene generated by RealTime PCR of serial dilutions of most concentrated DNA sample and appeared to be 94.7% for NADH dehydrogenase subunit 5, 94.5% for ATP synthase F0 subunit 6, and 81.2% for transferrin receptor. Quantities of target genes in the samples were estimated from RealTime PCR-generated C_t (cycle threshold) values corrected for amplification efficiency.

Statistical Analysis

Statistical analysis was performed using SigmaPlot 11.0 (SyStat Software, Chicago, IL). All results are expressed as mean \pm SEM. Comparisons between groups were performed with *t* test, ANOVA, or Kruskal-Wallis where appropriate. Differences were considered significant at a *p* value $< .05$.

RESULTS

At 4–7 months, $\text{Wrn}^{\Delta\text{hel}/\Delta\text{hel}}$ mice appeared healthy and in good condition; however at 14–16 months, the $\text{Wrn}^{\Delta\text{hel}/\Delta\text{hel}}$ mice had some grey fur and were beginning to develop bald patches. $\text{Wrn}^{\Delta\text{hel}/\Delta\text{hel}}$ mice were significantly heavier at 14–16 months than at 4–7 months (Figure 1); there were no differences in weight between the other groups.

Biochemical Parameters

Plasma insulin levels were increased in the $\text{Wrn}^{\Delta\text{hel}/\Delta\text{hel}}$ mice at both 4–7 months and 14–16 months of age compared

with 4- to 7-month-old WT. There was also an age-related increase in plasma insulin levels in the WT mice ($p = .014$, Figure 1B);

alanine transaminase, aspartate transaminase, and bilirubin levels in plasma were within the normal range in all age groups and genotypes (Figure 1C).

Morphological Studies

All livers from the 4- to 7-month-old and 14- to 16-month-old $\text{Wrn}^{\Delta\text{hel}/\Delta\text{hel}}$ and WT mice were free from pathological changes on hematoxylin and eosin staining (Figure 2A–D). However, a dramatic increase in inflammatory infiltrate was observed both in the 4- to 7-month-old and 14- to 16-month-old $\text{Wrn}^{\Delta\text{hel}/\Delta\text{hel}}$ mice compared with their age-matched controls (Figure 2A–D). Sirius red staining also revealed a significant increase in fibrotic changes in the parenchyma of the 4- to 7-month-old and 14- to 16-month-old $\text{Wrn}^{\Delta\text{hel}/\Delta\text{hel}}$ mice and parenchyma and vessels of the 14- to 16-month-old WT (Figure 2E–H).

Immunohistochemical Studies

ICAM 1 staining increased in both $\text{Wrn}^{\Delta\text{hel}/\Delta\text{hel}}$ age groups and in the 14- to 16-month-old WT group, reflecting the increased inflammation seen on histology (Figure 2I–L). In contrast, expression of LYVE-1, the marker for LSECs (Figure 2M–P), Perlecan, the marker for vascular extracellular matrix (Figure 2Q–T), and the Kupffer cell marker, F4/80 (Figure 2U–X) did not change with age or genotype.

Electron Microscopic Studies

Scanning electron microscopy revealed a significantly decreased number of fenestrations in 14- to 16-month-old WT mice and in both the 4- to 7-month-old and 14- to 16-month-old $\text{Wrn}^{\Delta\text{hel}/\Delta\text{hel}}$ mice ($p < .001$, Figure 3E). In addition, fenestration diameter was significantly decreased with age and genotype ($p = .004$, Figure 3F).

Transmission electron microscopy supported the histological findings of increased collagen deposition along the sinusoids in the space of Disse in the mice and more inflammatory cells in the sinusoids seen on light microscopy (Figure 4A–D). In addition, the hepatocytes were larger with age and genotype ($p = .001$, Figure 4A–D), and there were significantly increased levels of lipofuscin deposition in the 4- to 7-month-old $\text{Wrn}^{\Delta\text{hel}/\Delta\text{hel}}$ mice. Examination of the nucleus revealed an increase in irregularly shaped nuclei with $\text{Wrn}^{\Delta\text{hel}/\Delta\text{hel}}$ genotype (chi squared, 20.879, $p = .0001$, Figure 4I–L). There was no change in nuclei diameter ($\text{Wrn}^{\Delta\text{hel}/\Delta\text{hel}}$: 4–7 months, $8.269 \pm 0.312 \mu\text{m}$; 14–16 months, $9.365 \pm 0.35 \mu\text{m}$; WT: 4–7 months, $8.067 \pm 0.287 \mu\text{m}$; 14–16 months, $19.091 \pm 0.601 \mu\text{m}$, $p = .052$) or ploidy

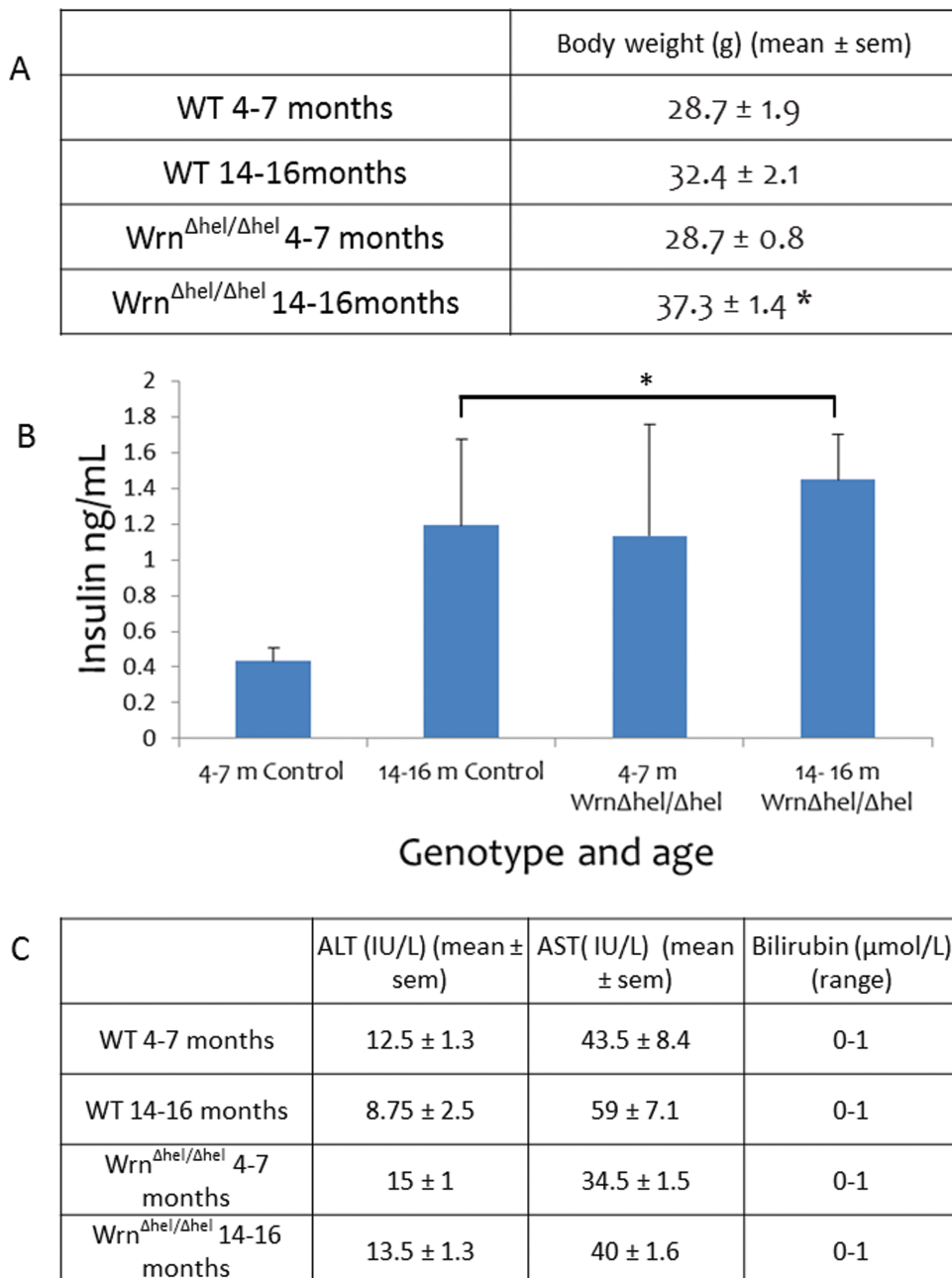


Figure 1. (A) Animal weight was significantly increased in the 14- to 16-month-old Wⁿ^{Δhel/Δhel} mice and WT mice compared with the 4- to 7-month-old animals ($p = .001$). (B) Hyperinsulinemia was seen in the progeroid 4- to 7-month-old Wⁿ^{Δhel/Δhel} mice and in both the WT and Wⁿ^{Δhel/Δhel} mice at 14–16 months (* $p = .014$). (C) No difference in liver function was detected between genotype and age.

(data not shown) with age or genotype. Localized fatty changes were found in the Wⁿ^{Δhel/Δhel} mice in both age groups (Figure 4I–L).

As assessed by maximal diameter measurements, there was an increase in hepatocyte mitochondrial size in the Wⁿ^{Δhel/Δhel} mice in both age groups compared with WT controls ($p = .004$, Figure 4E–H). In addition, there was a reduction in hepatocyte mitochondrial numbers per 100 μm^2 in both age groups of the Wⁿ^{Δhel/Δhel} mice and also in 14- to

16-month-old the WT control mice ($p = .036$, Figure 4N). The mitochondria appeared to be ultrastructurally normal in all groups, with cristae and membranes intact and uncompromised.

Mitochondrial Function Studies

Mitochondria extracted from the livers of 4- to 7-month-old WT and Wⁿ^{Δhel/Δhel} mice and analyzed using the Seahorse analyzer showed significant differences in: ADP-dependent

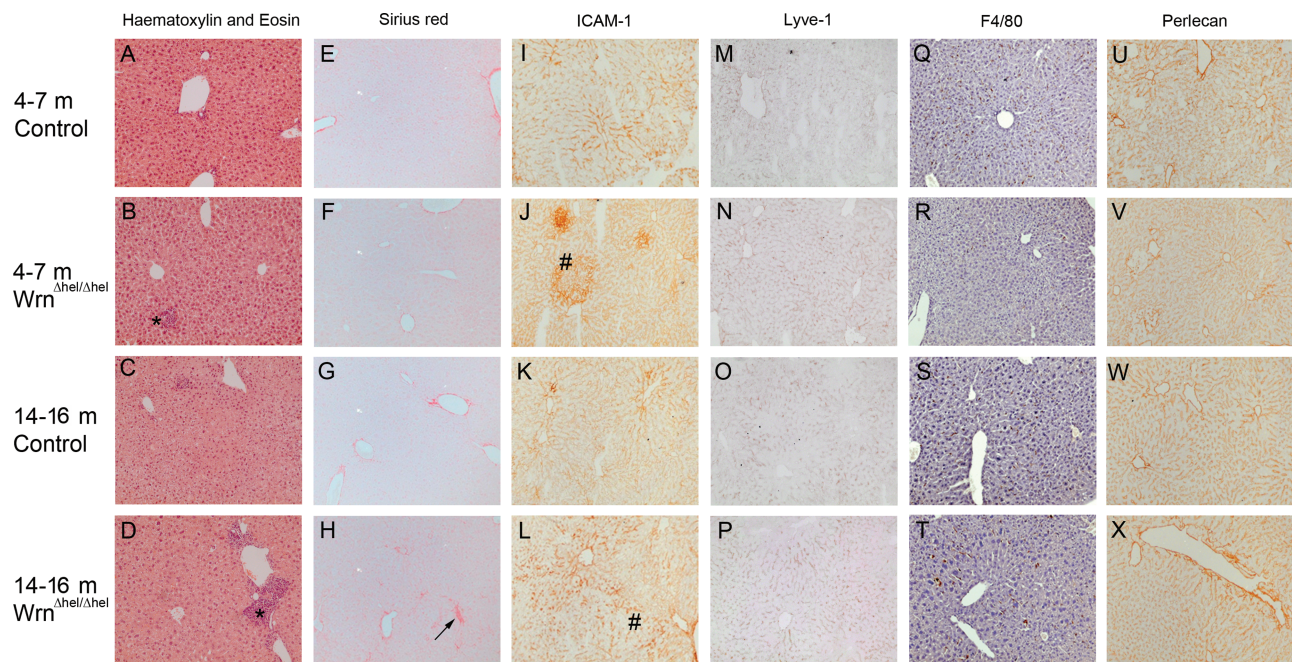


Figure 2. Histology and Immunohistochemistry of the liver. Hematoxylin and eosin staining of the liver (A–D) confirmed that although the livers of all mice were free of pathology, there is an increase in inflammatory cell aggregation (*) with age and *Wrn*^{Δhel/Δhel} genotype. Sirius red staining (E–H) revealed an increase in collagen deposition along the sinusoids with age (→) and *Wrn*^{Δhel/Δhel} genotype. Upregulation of ICAM-1 expression (#) (I–L) confirmed the hematoxylin and eosin finding of increased inflammation in the livers of *Wrn*^{Δhel/Δhel} and 14- to 16-month-old WT mice. No age- or genotype-dependent changes in expression of Lyve-1 (M–P), F4/80 (Q–T), or Perlecan (U–X) were detected. (Original magnification $\times 400$).

state III respiration ($p = .002$); ADP-independent state IV respiration ($p = .028$); and FCCP uncoupled respiration rates ($p = .001$). There were no differences in ADP:O ratio, a measure of overall ETC efficiency or hydrogen peroxide production (Figure 5A–F).

Mitochondrial DNA was quantified by measuring mtDNA copy numbers as measured by NADH dehydrogenase subunit 5 and ATP synthase F0 subunit 6 levels normalized against nuclear DNA copy numbers, measured by transferrin receptor; no significant difference was found in this parameter using this method of measurement (Figure 5G and H).

Microarray Studies

Gene regulation by both genotype and age was assessed using microarray in both hepatocytes and LSECs.

In LSECs, the scavenger receptor class A (Msrl) and transmembrane protein 66 (Tmem66) were both upregulated in the mutant mice, whereas the RNA-binding motif protein 13 (Rbm13) was significantly downregulated in *Wrn*^{Δhel/Δhel} LSECs (Figure 6A).

In hepatocytes, the WS homolog (human) (Wrn) and transmembrane protein 66 (Tmem66) were significantly upregulated, whereas RNA-binding motif protein 13 (Rbm13) and solute carrier family 7 (cationic amino acid transporter) member 2 (Slc-7a2) (Figure 6B) were significantly downregulated in the mutant mice. Of note,

expression patterns of Tmem66g and Rbm13 were very similar in LSECs and hepatocytes.

Age-dependent gene regulation.—Sixty-six genes were differentially regulated with age in LSECs independently of genotype. Figure 6C shows Gene Ontology terms statistically overrepresented within this list (Supplementary File). Aging was associated with significant upregulation of, for example, chemokine (C-X-C motif) ligand 12 (Cxcl12); arginine-rich domain-containing protein (Aard); collectin subfamily member 11 (Colec11); angiotensin II receptor, type 1a (Agtr1a); transmembrane protein 56 (Tmem56); and musculoskeletal, embryonic nuclear protein 1 (Mustn1) in both *Wrn*^{Δhel/Δhel} and WT animals although always to a lesser extent in the former.

No transcripts reached statistical significance for the age-related changes in hepatocytes when Benjamini–Hochberg false discovery rate correction was applied. However, when less strict statistical criteria were used, 513 transcripts were identified ($p < .005$). The Supplementary file shows the genes statistically overrepresented within this list. For example, aging was associated with significant upregulation of cell death-inducing DNA fragmentation factor; alpha subunit-like effector A (Cidea); CCR4 carbon catabolite repression 4-like (*Saccharomyces cerevisiae*) (Ccrn4l); glypican 1 (Gpc1); leucine-rich repeats and transmembrane domains 1 (Lrtm1); and WAP four-disulfide core domain 2

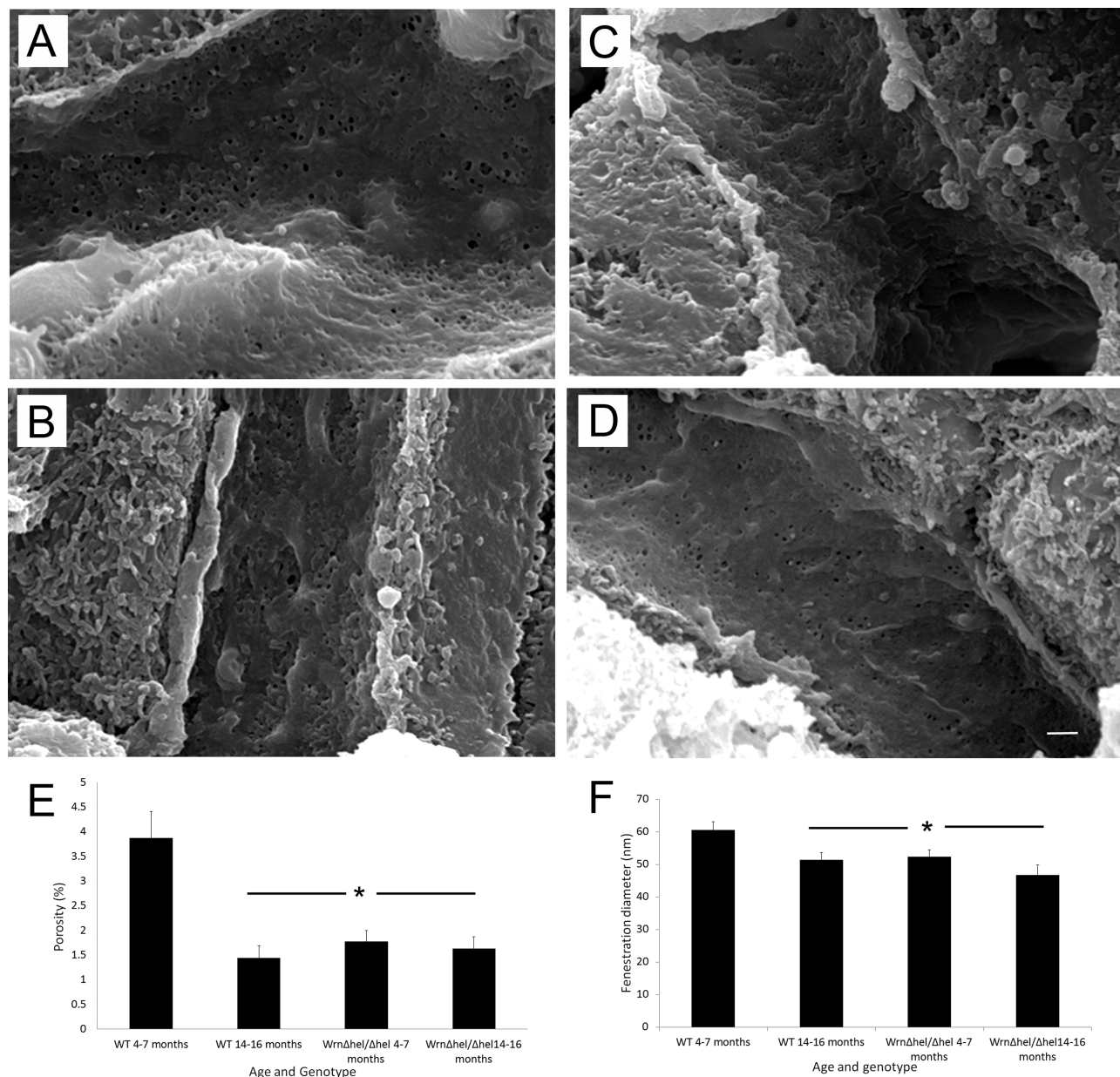


Figure 3. Scanning electron microscopy of the liver sinusoidal endothelium. (A–D) Typical scanning electron micrographs from 4- to 7-month-old WT, 4- to 7-month-old W^{nΔhel/Δhel}, 14- to 16-month-old WT, and 14- to 16-month-old W^{nΔhel/Δhel} mice, respectively. Reduced porosity and fenestration diameter in both age groups of the W^{nΔhel/Δhel} mice and 14- to 16-month-old WT mice. Figure 3E is quantification of the genotype- and age-related defenestration of the sinusoidal endothelium (* $p < .001$), and Figure 3F shows the decreased fenestration diameter (* $p = .004$). Original magnification $\times 15000$, Scale bar = 1 μm .

(Wfdc2) in both W^{nΔhel/Δhel} and WT hepatocytes. In contrast to LSECs, age-related upregulation of transcription was less pronounced in WT animals.

DISCUSSION

Ultrastructural changes during aging contribute to impaired liver metabolism and detoxification. Many of these changes occur in the hepatic blood vessels or sinusoids and occur independently of any disease pathology. In young disease-free liver, the hepatic sinusoids have a unique

fenestrated endothelium that allows bidirectional transfer of substances between the blood and the hepatocytes (26). However, during aging, a loss of fenestrations, an increase in extracellular matrix deposition, and changes in cell differentiation patterns impede transfer across the endothelium leading to impaired liver function and increased risk factors for adverse drug reactions and dyslipidemic conditions (7,24). This pattern of age-related changes in the liver sinusoid has been termed “pseudocapillarization.”

We have now demonstrated that the W^{nΔhel/Δhel} progeria model replicates age-related pseudocapillarization from

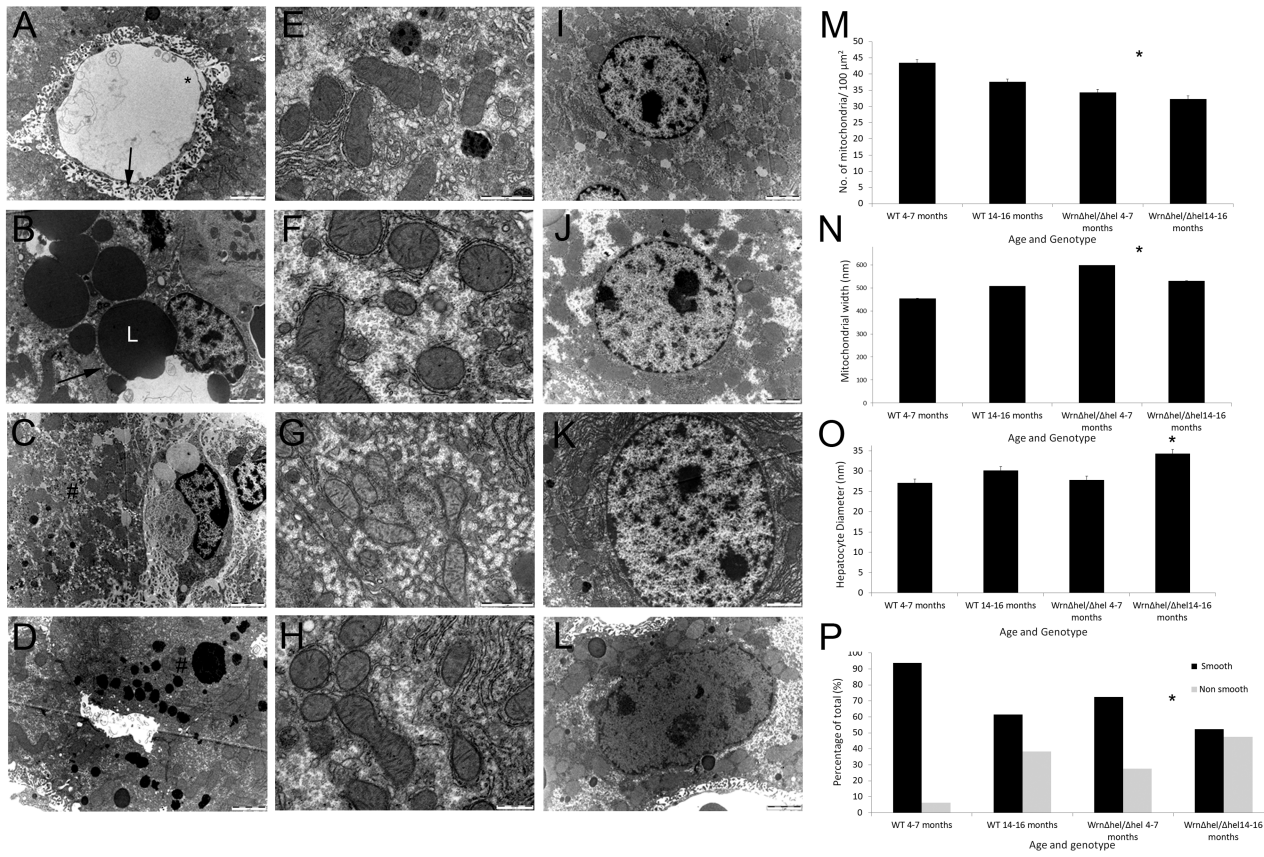


Figure 4. Transmission electron microscopy of the liver in $W\text{r}n^{\Delta\text{hel}/\Delta\text{hel}}$ and WT mice. (A) It depicts the liver of a 4- to 7-month-old WT mouse. The endothelium is fenestrated (*) and the space of Disse (→) is free from extracellular matrix deposition. (B) Micrograph taken from a 4- to 7-month-old $W\text{r}n^{\Delta\text{hel}/\Delta\text{hel}}$ mouse; there is significant lipid deposition (L) in the hepatocyte, and the space of Disse (→) has significant extracellular matrix deposition. Micrographs (C) and (D) are taken from 14- to 16-month-old WT and 14- to 16-month-old $W\text{r}n^{\Delta\text{hel}/\Delta\text{hel}}$ mice, respectively. The increased lipofuscin deposition seen in $W\text{r}n^{\Delta\text{hel}/\Delta\text{hel}}$ is clearly apparent (#). (E–H) They display the changes seen in mitochondrial number and size with age and genotype: in E, 4- to 7-month-old WT; F, 4- to 7-month-old $W\text{r}n^{\Delta\text{hel}/\Delta\text{hel}}$; G, 14- to 16-month-old WT; and H, 14- to 16-month-old $W\text{r}n^{\Delta\text{hel}/\Delta\text{hel}}$ mice. Changes in mitochondrial number per 100 μm^2 are quantified in M (* $p = .036$), and changes in mitochondrial diameter are shown in N (* $p = .004$). Changes in nuclear shape with age and genotype are seen in micrographs: I, 4- to 7-month-old WT; J, 4- to 7-month-old $W\text{r}n^{\Delta\text{hel}/\Delta\text{hel}}$; K, 14- to 16-month-old WT; and L, 14- to 16-month-old $W\text{r}n^{\Delta\text{hel}/\Delta\text{hel}}$ mice. Increases in maximal hepatocyte diameter with genotype and age are shown in O (* $p = .001$), and P displays the proportional increase in ruffled nuclei with genotype and age (* $p = .0001$). Scale bars as marked on the micrographs.

an early age. All animals included in this study are free from exogenously induced pathological changes as evidenced by the histological findings, liver enzyme levels, and gross morphological observations. The $W\text{r}n^{\Delta\text{hel}/\Delta\text{hel}}$ mice exhibit defenestration and decreased fenestration diameter (Figure 3) together with increased extracellular matrix (Figure 2) and changes in markers of LSEC inflammation, such as increased ICAM-1 expression and increased cell aggregates (Figure 2) from as early as 4–7 months. These changes are all hallmarks of the normal aging liver sinusoid and have been studied by numerous groups (27–32) since our original reporting in 2000 (33).

In addition to changes in the LSEC, there are changes in the hepatocytes of the $W\text{r}n^{\Delta\text{hel}/\Delta\text{hel}}$ mice. Hepatocytes are larger in the $W\text{r}n^{\Delta\text{hel}/\Delta\text{hel}}$ mice compared with WT control mice. In addition, the hepatocytes of $W\text{r}n^{\Delta\text{hel}/\Delta\text{hel}}$ mice have increased lipofuscin deposition, more frequent nuclear morphological anomalies, decreased mitochondria number, and increased mitochondrial diameter compared with WT

hepatocytes as evidenced by our electron microscopy analyses (34–36) (Figure 4). Such findings are typical of aging hepatocytes in many species (37).

The $W\text{r}n^{\Delta\text{hel}/\Delta\text{hel}}$ mice also have altered mitochondrial function as measured by the Seahorse technology (Figure 5A–F). The decreased number of mitochondrial organelles and the presence of larger mitochondria measured by electron microscopy in the $W\text{r}n^{\Delta\text{hel}/\Delta\text{hel}}$ mice reflect altered cell energy metabolism and are typical of aging mitochondria in many tissues. However, mtDNA copy number measurements (Figure 5G and H) were unchanged in the $W\text{r}n^{\Delta\text{hel}/\Delta\text{hel}}$ mice. The most likely reason for this is that a single mitochondrion can contain 2–10 copies of its DNA (38), and the decreased number of mitochondria in $W\text{r}n^{\Delta\text{hel}/\Delta\text{hel}}$ mice and in older 13- to 14-month-old WT mice could be compensated for by increased copies of DNA in the remaining mitochondria. In addition, Seahorse measurements of mitochondrial function showed increased respiration rate and uncoupling. Together the data indicate that mitochondrial function is altered in the

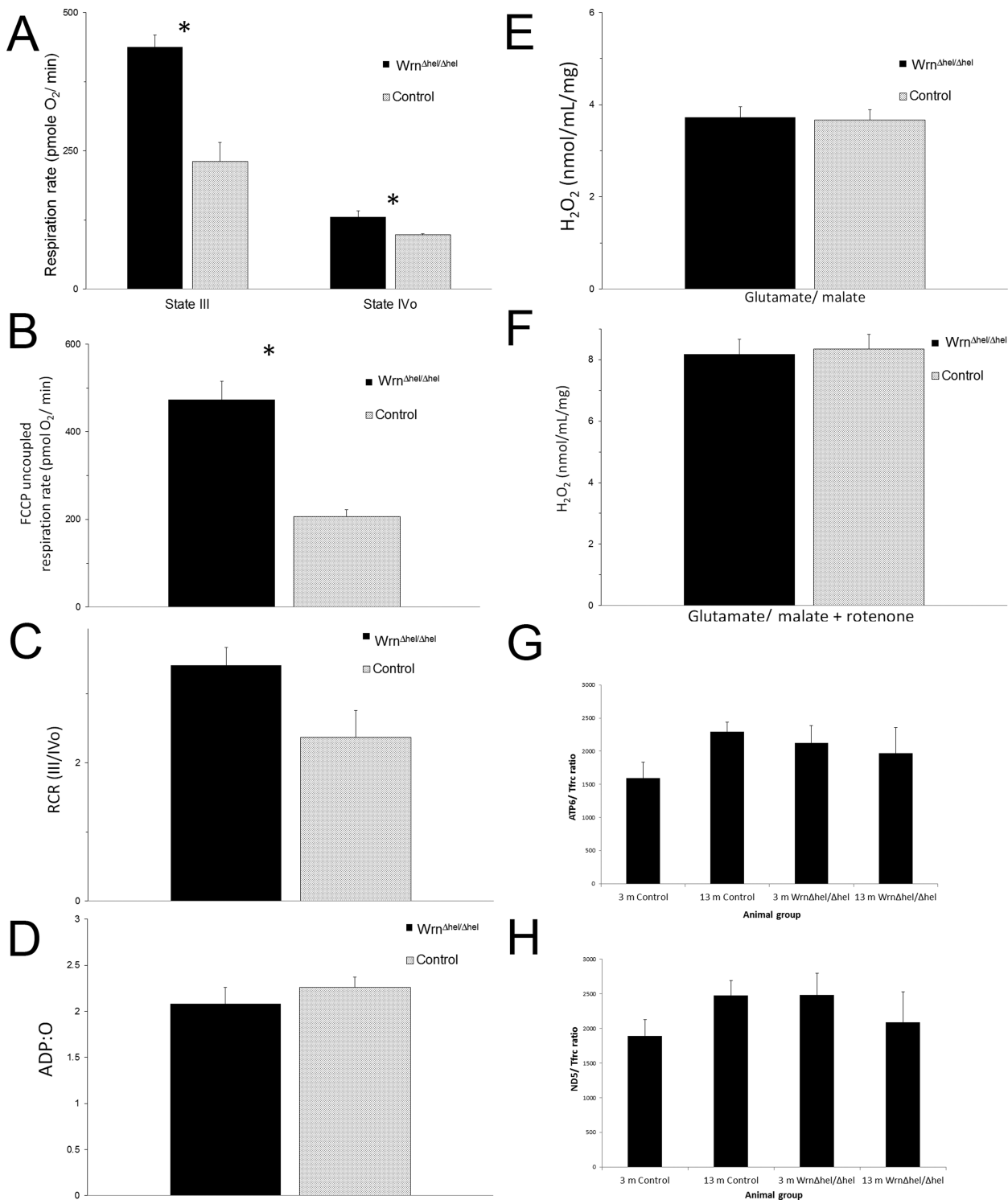


Figure 5. Mitochondrial function in $W^{n\Delta}\Delta^{hel}/\Delta^{hel}$ and control mice. Mitochondrial function as determined by Seahorse technology revealed significant loss of mitochondrial function in liver mitochondrial function in $W^{n\Delta}\Delta^{hel}/\Delta^{hel}$ mice. (A) It shows decreased State III and IV respiration (*State III: $p = .002$, State IV: $p = .028$) and (B) FCCP uncoupled respiration rate ($p = .001$) can be seen. (C) The ratio of respiration rates was not significant but shows a trend to reduction ($p = .067$). No changes in (D) ADP production or (E and F) H_2O_2 synthesis were detected. Quantification of mitochondrial DNA (G and H) was also performed, and no age- or genotype-dependent changes were found.

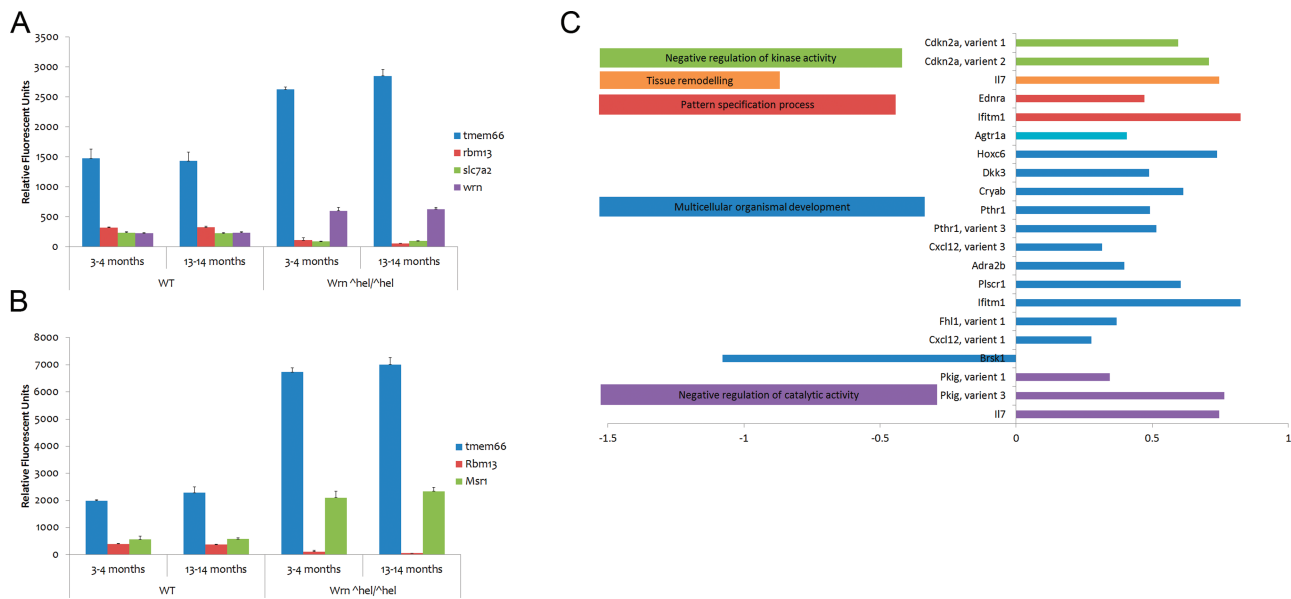


Figure 6. Significant LSEC and hepatocyte microarray results in $\text{Wrn}^{\Delta\text{hel}/\Delta\text{hel}}$ and WT mice. Differential expression of genes in LSECs are displayed in (A), whereas (B) displays those differentially expressed in $\text{Wrn}^{\Delta\text{hel}/\Delta\text{hel}}$ in hepatocytes. The classes of genes differentially regulated by age in LSECs are shown in (C).

$\text{Wrn}^{\Delta\text{hel}/\Delta\text{hel}}$ mice, leading to increased mitochondrial volume as a compensatory mechanism or as part of the pathological progeroid process.

Nuclei morphology was changed with $\text{Wrn}^{\Delta\text{hel}/\Delta\text{hel}}$ genotype and age, consisting of a shift from regular round-shaped nuclei in the 4- to 7-month-old control mice to irregularly shaped, invaginated nuclei in the progeric $\text{Wrn}^{\Delta\text{hel}/\Delta\text{hel}}$ mice and the 14- to 16-month-old controls. No change in nuclear ploidy or nuclei size was found, which agrees with a previous report in WS (39).

The increased insulin levels in the serum of $\text{Wrn}^{\Delta\text{hel}/\Delta\text{hel}}$ mice may be reflective of impaired insulin uptake in the liver of these animals. We speculate that this may be due to changes in their sinusoidal endothelium. Endothelial integrity affects insulin transfer into the liver as shown in the PDGF- α knockout mouse. Such mice exhibit an 80% increased insulin sensitivity that correlate with the substantially increased number of fenestrations (40).

The microarray data (Figure 6) revealed that the $\text{Wrn}^{\Delta\text{hel}/\Delta\text{hel}}$ genotype does not affect the expression of many genes within the isolated hepatocytes, with only four genes that are differentially expressed in the $\text{Wrn}^{\Delta\text{hel}/\Delta\text{hel}}$ mice. *TMEM66* gene expression, which encodes SARAF, a regulator of calcium entry into cells (41), is upregulated in $\text{Wrn}^{\Delta\text{hel}/\Delta\text{hel}}$ mice compared with WT mice (Figure 6B). *RBM13*, also known as MAK 16, is a RNA-binding protein involved in the stability and translation of RNA following stress and cell damage (42) and is downregulated (Figure 6C) in $\text{Wrn}^{\Delta\text{hel}/\Delta\text{hel}}$ mice compared with WT mice. In addition, *MSR-1*, which encodes the macrophage scavenger receptor-1, is upregulated in the LSECs of $\text{Wrn}^{\Delta\text{hel}/\Delta\text{hel}}$ mice. This protein is implicated in many physiological and

pathological conditions such as Alzheimer's disease, atherosclerosis, and cancers (43). It is believed to be implicated in NASH and several dyslipidemic liver conditions (44). Finally, *SLC-7a2* is downregulated in the hepatocytes of $\text{Wrn}^{\Delta\text{hel}/\Delta\text{hel}}$ mice. *SLC-7a2* encodes the solute carrier family 7 (cationic amino acid transporter) member 2, which is responsible for uptake of arginine, lysine, and ornithine. A dysfunction of this receptor has been shown to have implications in hyperinsulinemia (45) as seen in the $\text{Wrn}^{\Delta\text{hel}/\Delta\text{hel}}$ mice.

Microarray data also reveal that the LSEC is very susceptible to age-related changes in gene expression. No gene was differentially expressed across the age groups examined in the hepatocytes, whereas 66 genes were changed with age in the LSECs (Figure 6C).

Other progeroid mouse models have been created that recapitulate premature aging phenotypes (31,46–49). All models show abnormal nuclear morphology. The liver has been studied in the *Ercc*^{-Δ} mouse model, which shows pseudocapillarization, increased nuclear invagination, and lipofuscin deposits. The hepatocyte mitochondria were not studied in this model, but the observation of increased oxidative damage suggests mitochondrial dysfunctions (31). Although there are no comprehensive studies of the liver in the other progeroid syndrome models, lamin A/C gene mutations are associated with hyperlipidemia, hyperglycemia, and atherosclerosis (50), also suggestive of possible liver changes.

In summary, pseudocapillarization and other hallmarks of aging such as mitochondrial dysfunction are apparent from as early as 4 months of age in the $\text{Wrn}^{\Delta\text{hel}/\Delta\text{hel}}$ mice and resemble the phenotypic changes seen in the liver tissue of

much older WT animals. Progeria and aging changes were more remarkable in the LSEC than in the hepatocytes, confirming the importance of the sinusoidal cells in liver aging. As such, the *Wrn*^{Δhel/Δhel} model provides a valuable model for studying the important role the liver plays in aging.

SUPPLEMENTARY MATERIAL

Supplementary material can be found at: <http://biomedgerontology.oxfordjournals.org/>.

FUNDING

We acknowledge the financial support of the National Health and Medical Research Council (570937) and Ramaciotti Foundation (RN 23/08).

ACKNOWLEDGMENT

We gratefully acknowledge the contribution of Mamdouh Khalil of the Molecular Physiology unit, ANZAC Research Institute, Dorothy Kouzios of the Diagnostic Pathology unit, Concord Hospital and all members of the Electron Microscopy Unit at Concord Hospital. We thank Dr. Patrick Bertolino for his kind gift of the ICAM-1 and F4/80 antibodies. We acknowledge the financial support of the National Health and Medical Research Council and Ramaciotti Foundation.

REFERENCES

- Le Couteur DG, Cogger VC, Hilmer SN, et al. Aging, atherosclerosis and the liver sieve. In: Randall LO, ed. *Aging and the Elderly: Psychology, Sociology and Health*. New York: NOVA Science Publishers; 2006:153–176.
- Harman D. Aging: overview. *Ann NY Acad Sci*. 2001;928:1–21.
- Andrews GR, Khalil Z, Le Couteur DG. Experimental gerontological research in Australia. *Exp Gerontol*. 2002;37:1303–1310.
- Hilmer SN, Cogger VC, Le Couteur DG. Basal activity of Kupffer cells increases with old age. *J Gerontol A Biol Sci Med Sci*. 2007;62:973–978.
- Popper H. Aging and the liver. *Prog Liver Dis*. 1986;8:659–683.
- Le Couteur DG, Warren A, Cogger VC, et al. Old age and the hepatic sinusoid. *Anat Rec (Hoboken)*. 2008;291:672–683.
- Hilmer SN, Cogger VC, Fraser R, McLean AJ, Sullivan D, Le Couteur DG. Age-related changes in the hepatic sinusoidal endothelium impede lipoprotein transfer in the rat. *Hepatology*. 2005;42:1349–1354.
- Mitchell SJ, Huizer-Pajkoss A, Cogger VC, et al. Age-related pseudocapillarization of the liver sinusoidal endothelium impairs the hepatic clearance of acetaminophen in rats. *J Gerontol A Biol Sci Med Sci*. 2011;66:400–408.
- Kamath-Loeb AS, Shen JC, Loeb LA, Fry M. Werner syndrome protein. II. Characterization of the integral 3' → 5' DNA exonuclease. *J Biol Chem*. 1998;273:34145–34150.
- Shen JC, Gray MD, Oshima J, Kamath-Loeb AS, Fry M, Loeb LA. Werner syndrome protein. I. DNA helicase and dna exonuclease reside on the same polypeptide. *J Biol Chem*. 1998;273:34139–34144.
- Constantinou A, Tarsounas M, Karow JK, et al. Werner's syndrome protein (WRN) migrates Holliday junctions and co-localizes with RPA upon replication arrest. *EMBO Rep*. 2000;1:80–84.
- Opresko PL, Otterlei M, Graakjaer J, et al. The Werner syndrome helicase and exonuclease cooperate to resolve telomeric D loops in a manner regulated by TRF1 and TRF2. *Mol Cell*. 2004;14:763–774.
- Turaga RV, Paquet ER, Sild M, et al. The Werner syndrome protein affects the expression of genes involved in adipogenesis and inflammation in addition to cell cycle and DNA damage responses. *Cell Cycle*. 2009;8:2080–2092.
- Yamamoto K, Imakiire A, Miyagawa N, Kasahara T. A report of two cases of Werner's syndrome and review of the literature. *J Orthop Surg (Hong Kong)*. 2003;11:224–233.
- Goto M, Ishikawa Y, Sugimoto M, Furuichi Y. Werner syndrome: a changing pattern of clinical manifestations in Japan (1917~2008). *Biosci Trends*. 2013;7(1):13–22.
- Kitamoto T, Takemoto M, Fujimoto M, et al. Sitagliptin successfully ameliorates glycemic control in Werner syndrome with diabetes. *Diabetes Care*. 2012;35:e83.
- Lebel M, Leder P. A deletion within the murine Werner syndrome helicase induces sensitivity to inhibitors of topoisomerase and loss of cellular proliferative capacity. *Proc Natl Acad Sci USA*. 1998;95:13097–13102.
- Wang L, Ogburn CE, Ware CB, et al. Cellular Werner phenotypes in mice expressing a putative dominant-negative human WRN gene. *Genetics*. 2000;154:357–362.
- Lombard DB, Beard C, Johnson B, et al. Mutations in the WRN gene in mice accelerate mortality in a p53-null background. *Mol Cell Biol*. 2000;20:3286–3291.
- Lebel M, Lavoie J, Gaudreault I, Bronsard M, Drouin R. Genetic cooperation between the Werner syndrome protein and poly(ADP-ribose) polymerase-1 in preventing chromatid breaks, complex chromosomal rearrangements, and cancer in mice. *Am J Pathol*. 2003;162:1559–1569.
- Massip L, Garand C, Turaga RV, Deschênes F, Thorin E, Lebel M. Increased insulin, triglycerides, reactive oxygen species, and cardiac fibrosis in mice with a mutation in the helicase domain of the Werner syndrome gene homologue. *Exp Gerontol*. 2006;41:157–168.
- Labbe A, Garand C, Cogger VC, et al. Resveratrol improves insulin resistance hyperglycemia and hepatosteatosis but not hypertriglyceridemia, inflammation, and life span in a mouse model for Werner syndrome. *J Gerontol A Biol Sci Med Sci*. 2011;66:264–278.
- Massip L, Garand C, Paquet ER, et al. Vitamin C restores healthy aging in a mouse model for Werner syndrome. *FASEB J*. 2010;24:158–172.
- Cogger VC, Hilmer SN, Sullivan D, Muller M, Fraser R, Le Couteur DG. Hyperlipidemia and surfactants: the liver sieve is a link. *Atherosclerosis*. 2006;189:273–281.
- Huang Y, de Boer WB, Adams LA, et al. Image analysis of liver collagen using sirius red is more accurate and correlates better with serum fibrosis markers than trichrome. *Liver Int*. 2013;33:1249–1256.
- Cogger VC, Le Couteur DG. Fenestrations in the liver sinusoidal endothelial cell. In: Arias IM, Boyer JL, eds. *The Liver: Biology and Pathobiology*. Hoboken, NJ: John Wiley & Sons, Ltd; 2009, 387–404.
- Simon-Santamaría J, Malovic I, Warren A, et al. Age-related changes in scavenger receptor-mediated endocytosis in rat liver sinusoidal endothelial cells. *J Gerontol A Biol Sci Med Sci*. 2010;65:951–960.
- Tanaka T, Kono T, Terasaki F, et al. Thiamine prevents obesity and obesity-associated metabolic disorders in OLETF rats. *J Nutr Sci Vitaminol (Tokyo)*. 2010;56:335–346.
- Stacchiotti A, Lavazza A, Ferroni M, et al. Effects of aluminium sulphate in the mouse liver: similarities to the aging process. *Exp Gerontol*. 2008;43:330–338.
- Furrer K, Rickenbacher A, Tian Y, et al. Serotonin reverts age-related capillarization and failure of regeneration in the liver through a VEGF-dependent pathway. *Proc Natl Acad Sci USA*. 2011;108:2945–2950.
- Gregg SQ, Gutierrez V, Robinson AR, et al. A mouse model of accelerated liver aging caused by a defect in DNA repair. *Hepatology*. 2012;55:609–621.
- Ito Y, Sørensen KK, Bethea NW, et al. Age-related changes in the hepatic microcirculation in mice. *Exp Gerontol*. 2007;42:789–797.
- Le Couteur DG, Cogger VC, Markus AM, et al. Pseudocapillarization and associated energy limitation in the aged rat liver. *Hepatology*. 2001;33:537–543.
- Miquel J, Economos AC, Fleming J, Johnson JE Jr. Mitochondrial role in cell aging. *Exp Gerontol*. 1980;15:575–591.
- Schmucker DL, Sachs H. Quantifying dense bodies and lipofuscin during aging: a morphologist's perspective. *Arch Gerontol Geriatr*. 2002;34:249–261.

36. Andrew W. An electron microscope study of age changes in the liver of the mouse. *Am J Anat.* 1962;110:1–18.
37. Le Couteur DG, Sinclair DA, Cogger VC, et al. The aging liver and longterm caloric restriction. In: Everitt AV, Rattan SIS, Couteur DG, Cabo R, eds. *Calorie Restriction, Aging and Longevity*. Dordrecht, Netherlands; Springer Press; 2010:191–216.
38. Wiesner RJ, Rüegg JC, Morano I. Counting target molecules by exponential polymerase chain reaction: copy number of mitochondrial DNA in rat tissues. *Biochem Biophys Res Commun.* 1992;183:553–559.
39. Gahan PB, Middleton J. Euploidization of human hepatocytes from donors of different ages and both sexes compared with those from cases of Werner's syndrome and progeria. *Exp Gerontol.* 1984;19:355–358.
40. Raines SM, Richards OC, Schneider LR, et al. Loss of PDGF-B activity increases hepatic vascular permeability and enhances insulin sensitivity. *Am J Physiol Endocrinol Metab.* 2011;301:E517–E526.
41. Palty R, Raveh A, Kaminsky I, Meller R, Reuveny E. SARAF inactivates the store operated calcium entry machinery to prevent excess calcium refilling. *Cell.* 2012;149:425–438.
42. Abdelmohsen K, Srikanth S, Yang X, et al. Ubiquitin-mediated proteolysis of HuR by heat shock. *EMBO J.* 2009;28:1271–1282.
43. Bowdish DM, Gordon S. Conserved domains of the class A scavenger receptors: evolution and function. *Immunol Rev.* 2009;227:19–31.
44. Bieghs V, Verheyen F, van Gorp PJ, et al. Internalization of modified lipids by CD36 and SR-A leads to hepatic inflammation and lysosomal cholesterol storage in Kupffer cells. *PLoS One.* 2012;7:e34378.
45. González M, Flores C, Pearson JD, Casanello P, Sobrevia L. Cell signalling-mediated insulin increase of mRNA expression for cationic amino acid transporters-1 and -2 and membrane hyperpolarization in human umbilical vein endothelial cells. *Pflugers Arch.* 2004;448:383–394.
46. Wang Y, Herron AJ, Worman HJ. Pathology and nuclear abnormalities in hearts of transgenic mice expressing M371K lamin A encoded by an LMNA mutation causing Emery-Dreifuss muscular dystrophy. *Hum Mol Genet.* 2006;15:2479–2489.
47. Mounkes LC, Kozlov SV, Rottman JN, Stewart CL. Expression of an LMNA-N195K variant of A-type lamins results in cardiac conduction defects and death in mice. *Hum Mol Genet.* 2005;14:2167–2180.
48. Sullivan T, Escalante-Alcalde D, Bhatt H, et al. Loss of A-type lamin expression compromises nuclear envelope integrity leading to muscular dystrophy. *J Cell Biol.* 1999;147:913–920.
49. Arimura T, Helbling-Leclerc A, Massart C, et al. Mouse model carrying H222P-Lmna mutation develops muscular dystrophy and dilated cardiomyopathy similar to human striated muscle laminopathies. *Hum Mol Genet.* 2005;14:155–169.
50. Csoka AB, Cao H, Sammak PJ, Constantinescu D, Schatten GP, Hegele RA. Novel lamin A/C gene (LMNA) mutations in atypical progeroid syndromes. *J Med Genet.* 2004;41:304–308.